The EUMETSAT Satellite Application Facility on Land Surface Analysis (LSA SAF)

Algorithm Theoretical Basis Document (ATBD)

Land Surface Albedo

PRODUCTS: LSA-101 (MDAL), LSA-102 (MTAL), LSA-150 (MTAL-R)

Reference Number: **SAF/LAND/MF/ATBD_AL/1.1**
Issue/Revision Index: **Issue 1.1**
Last Change: **03/03/2014**

DOCUMENT SIGNATURE TABLE

	Name		
Prepared by :	**Météo-France / CNRM**	**04/03/2014**	
Approved by :	**Land SAF Project Manager**	**04/03/2014**	

DOCUMENTATION CHANGE RECORD

Issue / Revision	Date	Description:
Version 1.0	**09/11/2012**	
Version 1.1	**04/03/2014**	

DISTRIBUTION LIST

Internal Consortium Distribution		
Organization	**Name**	**No. Copies**
IM	Luís Pessanha	
IM	Isabel Trigo	
IDL	Carlos da Camara	
IM	Isabel Monteiro	
IM	Sandra Coelho	
IM	Carla Barroso	
IM	Pedro Diegues	
IM	Teresa Calado	
IM	Benvinda Barbosa	
IM	Ana Veloso	
IMK	Folke-S. Olesen	
IMK	Frank Goettsche	
IMK	Ewa Kabsch	
MF	Jean-Louis Roujean	
MF	Xavier Ceamanos	
MF	Dominique Carrer	
RMI	Françoise Meulenberghs	
RMI	Arboleda Alirio	
RMI	Nicolas Ghilain	
FMI	Niilo Siljamo	
UV	Joaquin Melia	
UV	F. Javier García Haro	
UV/EOLAB	Fernando Camacho	
UV	Aleixander Verger	

External Distribution		
Organization	**Name**	**No. Copies**
EUMETSAT	Frédéric Gasiglia	
EUMETSAT	Dominique Faucher	
EUMETSAT	Lorenzo Sarlo	
EUMETSAT	Lothar Schueller	
EDISOFT	Teresa Cardoso	
EDISOFT	Carlos Vicente	
EDISOFT	Cleber Balan	
SKYSOFT	Rui Alves	
SKYSOFT	João Canário	

Steering Group Distribution		
Nominated by:	**Name**	**No. Copies**

IM	**Carlos Direitinho Tavares**	
EUMETSAT	**Lorenzo Sarlo**	
EUMETSAT	**François Montagner**	
STG/AFG (USAM)	**Luigi de Leonibus**	
MF	**François Bouyssel**	
RMI	**Piet Termonia**	
FMI	**Carl Fortelius**	

Table of Contents

List of Figures

List of Tables

1 The EUMETSAT SAF on Land Surface Analysis

The EUMETSAT (European organization for the Exploitation of Meteorological Satellites) Satellite Application Facility (SAF) on Land Surface Analysis (LSA; Trigo et al., 2010) is part of the SAF Network, a set of specialized development and processing centers, serving as EUMETSAT distributed Applications Ground Segment. The SAF network complements the product-oriented activities at the EUMETSAT Central Facility in Darmstadt, Germany. The main purpose of the LSA SAF is to take full advantage of remotely sensed data to measure land surface variables, which will primarily find applications in meteorology (http://landsaf.meteo.pt/).

Several studies have stressed the role of land surface processes on weather forecasting and climate modeling (e.g., Dickinson et al., 1983; Mitchell et al., 2004; Ferranti and Viterbo, 2006). The LSA SAF has been especially designed to serve the needs of the meteorological community, particularly Numerical Weather Prediction (NWP). However, LSA SAF addresses other communities including users from:

- Weather forecasting and climate modeling, requiring detailed information on the nature and properties of land.
- Environmental management and land use, needing information on land cover type and land cover changes (e.g., provided by biophysical parameters or thermal characteristics).
- Agricultural and forestry applications, requiring information on incoming/outgoing radiation and vegetation properties.
- Renewable energy resources assessment, particularly biomass, depending on biophysical parameters, and solar energy.
- Natural hazards management, requiring frequent observations of terrestrial surfaces in both the solar and thermal bands.
- Climatological applications and climate change detection, requiring long and homogeneous time-series.

The LSA SAF exploits data acquired in the framework of two EUMETSAT missions, namely, the Meteosat Second Generation (MSG) platform and the Meteorological-Operational (Metop) satellites. Nowadays, only MSG-derived products are delivered to the scientific community. The spin-stabilized MSG spacecraft has an imaging-repeat cycle of 15 minutes. The SEVIRI radiometer embarked on the MSG platform encompasses unique spectral characteristics and accuracy, with a 3 km resolution (sampling distance) at nadir (1 km for the high-resolution visible channel), and 12 spectral channels (Schmetz et al., 2002) along the visible, the near-infrared, and the thermal infrared ranges (i.e., 0.6-13.4 μm). AL products of the LSA SAF are computed from level 1.5 SEVIRI data corresponding the short-wave channels at 0.6 μm (VIS1), 0.8 μm (VIS2) and 1.6 μm (NIR).

As shown in Figure 1, most products derived from SEVIRI/MSG such as AL are generated at full spatial resolution (3 km/pixel sampling distance at nadir), for 4 different geographical areas within MSG disk:

- Euro – Europe, covering all EUMETSAT member states;
- NAfr – Northern Africa encompassing the Sahara and Sahel regions, and part of equatorial Africa.
- SAfr – Southern Africa covering the African continent south of the Equator.
- SAme – South American continent within the MSG disk.

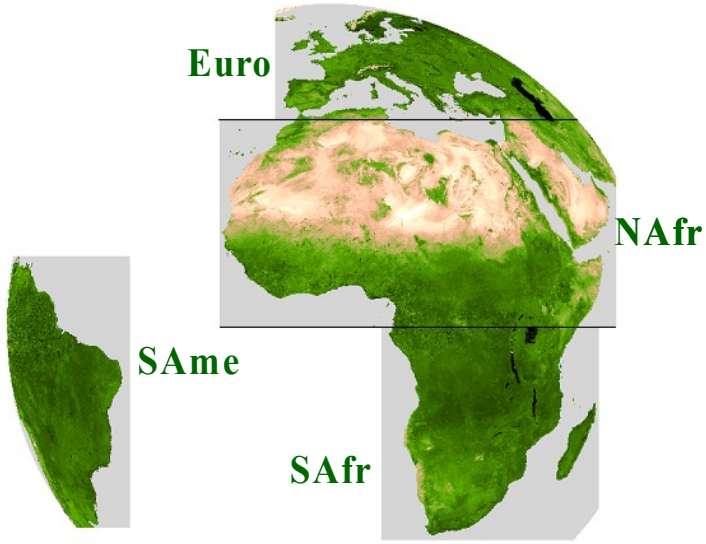

Figure 1 - The LSA SAF geographical areas for SEVIRI based products.

The LSA SAF products are summarized in Table 1. All LSA SAF products are validated regularly against ground measurements, model outputs, or similar parameters retrieved from other sensors. Furthermore, each retrieved value is distributed with a quality flag and/or error bar providing a qualitative/quantitative measure of the expected accuracy. The LSA SAF products are currently available from LSA SAF website (http://landsaf.meteo.pt) that contains real time examples of the products as well as updated information.

This document details the algorithm used for the retrieval of Land Surface Albedo (AL) from the Spinning Enhanced Visible and Infrared Imager (SEVIRI) onboard Meteosat Second Generation (MSG) satellites. The sections below describe the theoretical basis for AL estimation, together with the processing of the respective error budget. The methodology detailed here applies to near real time AL products – MDAL with product identifier LSA-101 & MTAL with product identifier LSA-102 – as well as to the re-processed AL dataset – MTAL-R with product identifier LSA-150.

Table 1 - Summary of LSA SAF operational or under-development products. Temporal resolution specifies the time interval to which the product applies.

Product Family	Product Group	Sensors/Platforms
Radiation	Land Surface Temperature (LST)	SEVIRI/MSG, AVHRR/Metop, FCI/MTG, VII/EPS-SG
	Land Surface Emissivity (EM)	SEVIRI/MSG, FCI/MTG (internal product for other sensors)
	Land Surface Albedo (AL)	SEVIRI/MSG, AVHRR/Metop, FCI/MTG, VII/EPS-SG, 3MI/EPS-SG
	Down-welling Short-wave Fluxes (DSSF)	SEVIRI/MSG, FCI/MTG
	Down-welling Long-wave Fluxes (DSLF)	SEVIRI/MSG, FCI/MTG
Vegetation	Normalized Difference Vegetation Index (NDVI)	AVHRR/Metop, VII/EPS-SG
	Fraction of Vegetation Cover (FVC)	SEVIRI/MSG, AVHRR/Metop, FCI/MTG, VII/EPS-SG, 3MI/EPS-SG
	Leaf Area Index (LAI)	SEVIRI/MSG, AVHRR/Metop, FCI/MTG, VII/EPS-SG, 3MI/EPS-SG
	Fraction of Absorbed Photosynthetically Active Radiation (FAPAR)	SEVIRI/MSG, AVHRR/Metop, FCI/MTG, VII/EPS-SG, 3MI/EPS-SG
	Gross Primary Production (GPP)	SEVIRI/MSG, FCI/MTG
	Canopy Water Content (CWC)	AVHRR/Metop, VII/EPS-SG
Energy Fluxes	Evapotranspiration (ET)	SEVIRI/MSG, FCI/MTG
	Reference Evapotranspiration (ET0)	SEVIRI/MSG, FCI/MTG
	Surface Energy Fluxes: Latent and Sensible (LE&H)	SEVIRI/MSG, FCI/MTG
Wild Fires	Fire Detection and Monitoring (FD&M)	SEVIRI/MSG
	Fire Radiative Power	SEVIRI/MSG, FCI/MTG, VII/EPS-SG
	Fire Radiative Energy and Emissions (FRE)	SEVIRI/MSG, FCI/MTG, VII/EPS-SG
	Fire Risk Map (FRM)	SEVIRI/MSG, FCI/MTG
	Burnt Area (BA)	AVHRR/Metop, VII/EPS-SG

2 Introduction

Land surface albedo (AL) is a key variable for characterizing the energy balance in the coupled surface-atmosphere system and constitutes an indispensable input quantity for soil-vegetation-atmosphere transfer models. As a matter of fact, land surface albedo quantifies the fraction of energy reflected by the surface of the Earth. As a corollary, AL also determines the fraction of energy absorbed by the surface and transformed into heat or latent energy.

Owing to strong feedback effects, the knowledge of surface albedo is also crucial for determining atmospheric conditions in the boundary layer. As Numerical Weather Prediction models become more sophisticated, it will become increasingly important to accurately describe the spatial and temporal albedo variations. On longer timescales, studies carried out with Global Circulation Models have revealed the sensitivity of climate with respect to changes in surface albedo.

The largest surface albedo changes are caused by snow fall. Snow characteristics and duration of snow cover have a direct impact on the environmental system. The seasonal monitoring of snow therefore is an important subject for numerical weather prediction, climate studies, and hydrology. Snow albedo varies with environmental conditions, land cover, and snow metamorphism. One of the objectives of the delivered product is to quantify the albedo changes on small timescales.

The most relevant albedo quantity for applications related to the energy budget refers to the total short-wave broad-band interval comprising the visible and near infrared wavelength ranges where the solar down-welling radiation dominates. In more refined models the albedo values in the visible and near infrared broad-band ranges may also be exploited separately. Estimates for the normalized the LSA SAF algorithm also delivers reflectance factor values and the spectral albedo in the satellite instrument channels. In addition to serving as an intermediate product for deriving the broad-band albedo quantities, the spectral estimates contain a wealth of information about the physical state of the surface. This information can be used for a variety of purposes such as vegetation monitoring and land cover classification, which in turn also constitute important elements for setting up adequate surface modeling schemes.

A well-established approach for operational albedo determination is based on semi-empirical BRDF (bidirectional reflectance distribution function) kernel models which have received a great deal of attention and effort from the optical remote sensing community in the last decades (e.g., Roujean et al., 1992; Barnsley et al., 1994; Wanner et al., 1995; Strahler, 1994; and Hu et al., 1997). The approach is based on a decomposition of the bi-directional reflectance factor into a number of kernel functions which are associated to dominant light scattering processes, for example, geometric and volumetric effects, separation between soil and vegetation contributions, or the conjunction between media which are optically thick and thin (Lucht and Roujean, 2000). Both in situ measurements and numerical experiments have supported this assumption and the use of kernel-based models is nowadays widely accepted since they yield a pragmatic and cost-effective solution to the problem of BRDF inversion. For a number of space-borne sensors of the current

generation of multi-angular systems the kernel-based approach was adopted for the development of albedo products. These include POLDER, SeaWiFS, VEGETATION, and MODIS (e.g., Leroy et al., 1997; Justice et al., 1998; Wanner et al., 1997; Strahler et al., 1999). On the other hand, different parametrized models and a simultaneous modeling of atmosphere and surface properties were considered for MISR (Diner et al., 1998) and Meteosat (Pinty et al., 2000a-b). The common feature of these algorithms is the correction and exploitation of the variations in sun-sensor geometry that occur as a function of satellite orbit, sensor design, geographical position of the target, and time of the year.

The Land Surface Albedo product of the LSA-SAF is produced from data acquired by the Spinning Enhanced Visible and Infrared Imager (SEVIRI) radiometer embarked on MSG. In the future, this product will be produced for the Advanced Very High Resolution Radiometer (AVHRR) aboard the series of Metop satellites. Forecasts provided by the European Center for Medium-range Weather Forecasts (ECMWF) are used as ancillary data for the atmospheric correction prior to the estimation of the AL products.

The present document is one of the product manuals dedicated to LSA SAF users. The algorithm theoretical basis of the land surface albedo generated by the LSA SAF are described in the following sections. The characteristics of the AL products derived from SEVIRI and provided by the LSA SAF are described in Table 2. Further details on the AL product requirements may be found in the Product Requirements Document (PRD) and the Product User Manual (PUM) which are available on the LSA SAF website.

Table 2 - Product Requirements for AL, in terms of area coverage, resolution and accuracy.

Product Name	Product Identifier	Coverage	Resolution		Accuracy		
			Temporal	Spatial	Threshold	Target	Optimal
MDAL (AL SEVIRI)	LSA-01	MSG disk	1 day	MSG pixel resolution	20%	AL>0.15:20% AL<0.15:0.03	7.5%
MTAL (AL SEVIRI)	LSA-02	MSG disk	10-day	MSG pixel resolution	10%	AL>0.15:10% AL<0.15: 0.015	5%

3 Theoretical framework

The spectral albedo of a plane surface is defined as the ratio between the hemispherical integrals of the up-welling (reflected) spectral radiance $L^{\uparrow}(\lambda,\theta_{out},\varphi_{out})$ and the down-welling spectral radiance $L^{\downarrow}(\lambda,\theta_{in},\varphi_{in})$ weighted by the cosine of the angle between the respective reference direction and the surface normal:

$$a(\lambda):=\frac{\int_{2\pi} L^{\uparrow}(\lambda,\theta_{out},\varphi_{out})\cos\theta_{out}\, d\Omega_{out}}{\int_{2\pi} L^{\downarrow}(\lambda,\theta_{in},\varphi_{in})\cos\theta_{in}\, d\Omega_{in}} \quad , \tag{1}$$

where $d\Omega_{out}=\sin\theta_{out}\, d\theta_{out}\, d\varphi_{out}$ and $d\Omega_{in}=\sin\theta_{in}\, d\theta_{in}\, d\varphi_{in}$. In other words, the term in the denominator defines the spectral solar irradiance $E^{\downarrow}(\lambda)$. By introducing the bi-directional reflectance factor R, the up-welling radiance distribution can be expressed in terms of the down-welling radiation as

$$L^{\uparrow}(\lambda,\theta_{out},\varphi_{out})=\frac{1}{\pi}\int_{2\pi} R(\lambda,\theta_{out},\varphi_{out},\theta_{in},\varphi_{in})\, L^{\downarrow}(\lambda,\theta_{in},\varphi_{in})\cos\theta_{in}\, d\Omega_{in} \quad , \tag{2}$$

and Equation (1) becomes

$$a(\lambda)=\frac{\frac{1}{\pi}\int_{2\pi}\int_{2\pi} R(\lambda,\theta_{out},\varphi_{out},\theta_{in},\varphi_{in})\, L^{\downarrow}(\lambda,\theta_{in},\varphi_{in})\cos\theta_{in}\cos\theta_{out}\, d\Omega_{in}\, d\Omega_{out}}{E^{\downarrow}(\lambda)} \quad . \tag{3}$$

It can be seen from the last equation that the spectral albedo of non-Lambertian surfaces generally depends on the angular distribution of the incident radiation, which in turn depends on the concentration and properties of scattering agents (e.g., aerosols) in the atmosphere and, in particular, on the presence of clouds. Therefore the spectral albedo is not a true surface property but rather a characteristic of the coupled surface-atmosphere system.

In the idealized case of totally direct illumination at incidence angles (θ_{dh} , φ_{dh}), the down-welling radiance is given by $L^{\downarrow}(\lambda,\theta_{in},\varphi_{in})=(\sin\theta_{dh})^{-1}\,\delta(\theta_{in}-\theta_{dh},\varphi_{in}-\varphi_{dh})E_0(\lambda)$, which results in $E^{\downarrow}(\lambda)=E_0(\lambda)\cos\theta_{dh}$ and

$$L^{\uparrow}(\lambda,\theta_{out},\varphi_{out};\theta_{dh},\varphi_{dh})=\frac{1}{\pi}R(\lambda,\theta_{out},\varphi_{out},\theta_{dh},\varphi_{dh})E_0(\lambda)\cos\theta_{dh} \quad . \tag{4}$$

By inserting these expressions into Equation (3) we obtain the spectral directional-hemispherical (or “black-sky”) albedo $a^{dh}(\lambda;\theta_{dh},\varphi_{dh})$:

$$a^{dh}(\lambda;\theta_{dh},\varphi_{dh})=\frac{1}{\pi}\int_{2\pi} R(\lambda,\theta_{out},\varphi_{out},\theta_{dh},\varphi_{dh})\cos\theta_{out}\, d\Omega_{out} \quad . \tag{5}$$

On the other hand, in the case of completely diffuse illumination the down-welling radiance $L^{\downarrow}(\lambda,\theta_{in},\varphi_{in})=L_0(\lambda)$ is constant and the solar irradiance becomes $E^{\downarrow}(\lambda)=\pi\, L_0(\lambda)$. By inserting these terms into Equation (3) and after making use of

Equation (5) the spectral bi-hemispherical (or "white-sky") albedo $a^{bh}(\lambda)$ can be written as:

$$a^{bh}(\lambda)=\frac{1}{\pi}\int_{2\pi} a^{dh}(\lambda;\theta_{in},\varphi_{in})\cos\theta_{in}\,d\,\Omega_{in} \quad . \tag{6}$$

These two quantities are true surface properties and correspond to the limiting cases of point source ($a^{dh}(\lambda;\theta_{dh},\varphi_{dh})$) and completely diffuse illumination ($a^{bh}(\lambda)$). For partially diffuse illumination the actually occurring spectral albedo value may be approximated as a linear combination of the limiting cases

$$a(\lambda)\approx[1-f_{diffuse}(\lambda)]a^{dh}(\lambda;\theta_s,\varphi_s)+f_{diffuse}(\lambda)a^{bh}(\lambda)\ , \tag{7}$$

where $f_{diffuse}$ denotes the fraction of diffuse radiation and (θ_s , φ_s) the solar direction.

For many applications the quantity of interest is not the spectral, or narrow-band, but rather the broad-band albedo which is defined as the ratio of up-welling to down-welling radiation fluxes in a given wavelength interval [λ_1 , λ_2]:

$$a_{[\lambda_1,\lambda_2]}:=\frac{F^{\uparrow}_{[\lambda_1,\lambda_2]}}{F^{\downarrow}_{[\lambda_1,\lambda_2]}}=\frac{\int_{\lambda_1}^{\lambda_2}\int_{2\pi} L^{\uparrow}(\lambda,\theta_{out},\varphi_{out})\cos\theta_{out}\,d\,\Omega_{out}\,d\lambda}{\int_{\lambda_2}^{\lambda_2}\int_{2\pi} L^{\downarrow}(\lambda,\theta_{in},\varphi_{in})\cos\theta_{in}\,d\,\Omega_{in}\,d\lambda} \quad . \tag{8}$$

In analogy to Equation (3) it can be expressed in terms of the bi-directional reflectance factor as

$$a(\lambda)=\frac{\frac{1}{\pi}\int_{\lambda_1}^{\lambda_2}\int_{2\pi}\int_{2\pi} R(\lambda,\theta_{out},\varphi_{out},\theta_{in},\varphi_{in})L^{\downarrow}(\lambda,\theta_{in},\varphi_{in})\cos\theta_{in}\cos\theta_{out}\,d\,\Omega_{in}\,d\,\Omega_{out}\,d\lambda}{F^{\downarrow}_{[\lambda_1,\lambda_2]}} \quad . \tag{9}$$

In this case the directional-hemispherical broad-band albedo

$$a^{dh}_{[\lambda_1,\lambda_2]}(\theta_{dh},\varphi_{dh})=\frac{\int_{\lambda_1}^{\lambda_2} a^{dh}(\lambda;\theta_{dh},\varphi_{dh})E^{\downarrow}(\lambda)\,d\lambda}{\int_{\lambda_1}^{\lambda_2} E^{\downarrow}(\lambda)\,d\lambda}\ , \tag{10}$$

and the bi-hemispherical broad-band albedo

$$a^{bh}_{[\lambda_1,\lambda_2]} = \frac{\int_{\lambda_1}^{\lambda_2} a^{bh}(\lambda) E^{\downarrow}(\lambda)\, d\lambda}{\int_{\lambda_1}^{\lambda_2} E^{\downarrow}(\lambda)\, d\lambda}\,, \qquad (11)$$

can be written as integrals of the respective spectral quantities weighted by the spectral irradiance. The corresponding broad-band albedo values are not pure surface properties since the wavelength dependence of the spectral irradiance $E(\lambda)$ appearing as a weight factor in their definition may vary as a function of the atmospheric composition. In analogy to Equation (7) the broad-band albedo for partially diffuse illumination conditions may be expressed as a weighted average of $a^{dh}_{[\lambda_1,\lambda_2]}(\theta_s,\varphi_s)$ and $a^{bh}_{[\lambda_1,\lambda_2]}$.

4 Algorithm description

4.1 Overview

Satellite observations provide TOA radiance measurements for certain configurations of illumination and observation geometry. The calculation of surface albedo according to the equations above requires the knowledge of the complete bi-directional reflectance distribution function of the surface. To obtain an estimate of this quantity it is necessary to solve the radiative transfer problem in the coupled surface-atmosphere system. In the LSA SAF system a simplified approach is adopted. In a first step an atmospheric correction is performed in order to derive top-of-canopy (TOC) reflectance values corresponding to the occurring angular observation configurations. In the second step of the LSA SAF system a semi-empirical kernel-based reflectance model is adjusted to the measurements. This delivers an estimate of the complete angular dependence of the bi-directional reflectance factor R_β in the spectral channel β of the measuring instrument:

$$R_\beta(\theta_{out}, \theta_{in}, \varphi) = \mathbf{k}_\beta \mathbf{f}(\theta_{out}, \theta_{in}, \varphi) \quad . \tag{12}$$

Here $\mathbf{k}_\beta = (k_{0\beta}, k_{1\beta}, k_{2\beta}, \ldots)^T$ and $\mathbf{f} = (f_0, f_1, f_2, \ldots)^T$ represent vectors formed by the retrieved model parameters $k_{i\beta}$ and the kernel functions f_i, respectively. The individual azimuth angles were replaced by the relative azimuth angle φ between the directions of incoming and outgoing light paths. This is possible without restriction of generality as long as the surface is considered as spatially isotropic.

The proposed algorithm consists in calculating the “black-sky” a_β^{dh} and “white-sky” a_β^{bh} albedos defined by integrals (5) and (6) in all instrument channels β by using the coefficients $\mathbf{k}_\beta$ provided by the directional reflectance model inversion. The narrow-band albedo values serve as an approximation to the spectral albedo at the central band wavelength λ_β. Furthermore broad-band albedo values a_γ^{dh} and a_γ^{bh} corresponding to suitable intervals $\gamma = [\lambda_1, \lambda_2]$ are derived from the spectral estimates by employing appropriate approximations to the integrals (10) and (11).

The operational processing scheme of the LSA SAF albedo algorithm is depicted in the flow chart of Figure 3 and comprises the following four successive steps:

1. First the measured top-of-atmosphere (TOA) radiances delivered by the satellite instrument are corrected for atmospheric effects in order to convert them into the corresponding TOC reflectance values.
2. The spectral TOC reflectances then serve as the input quantities for the inversion of a linear kernel-driven BRDF model, which allows us to take into account the angular dependence of the reflectance factor.
3. Spectral albedo values in the instrument channels are determined from the angular integrals of the model functions with the retrieved parameter values.
4. Finally, a narrow to broad-band conversion is performed with a linear regression formula.

Technically speaking the processing chain comprises two distinct modules, one for atmospheric correction and one for model inversion and directional and spectral integration. The atmospheric correction module is applied separately on each SEVIRI image available at intervals of 15 minutes directly after acquisition. The inversion and albedo calculation module, on the other hand, operates on a set of images in TOC reflectance units collected during one day. By using the previous inversion result as a priori information, a recursive temporal composition of the information over a longer time period can be achieved in order to guarantee the coherence and spatial completeness of the product.

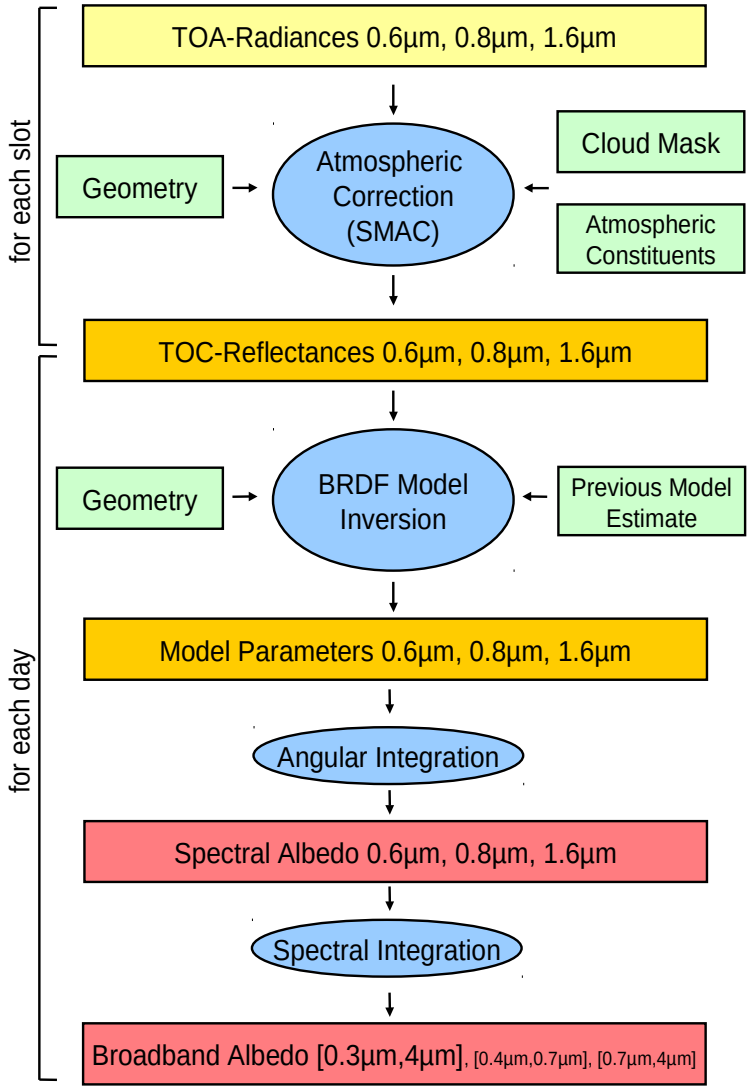

Figure 2: Flow chart of the algorithm for atmospheric correction, BRDF model inversion, and albedo determination.

4.2 Atmospheric correction

The LSA SAF operational system provides TOA radiances as well as all auxiliary information needed to perform atmospheric correction at the temporal resolution of the image acquisition and the spatial resolution of the SEVIRI instrument. The required quantities include the illumination and observation angles, a land/water-mask, the cloud-mask product (CMa) generated with software components developed by the Nowcasting-SAF, surface pressure information obtained from the ECMWF numerical weather prediction model combined with the use of a digital elevation model, column water vapor from the ECMWF model, and ozone content estimated by using the TOMS climatology.

The measurements of the TOA radiance $\hat{L}_\beta$ in the spectral channels of the SEVIRI instrument are first converted to TOA reflectance factor values:

$$\hat{R}_\beta = \frac{\hat{L}_\beta}{B_\beta \, v(t) \cos\theta_s} \quad . \tag{13}$$

The band factor B_β depends on the solar spectral irradiance and the spectral sensitivity of the respective channel (Derrien, 2002). The numerical values currently used are 20.76 mW/(m^2 sr cm^{-1}), 23.24 mW/(m^2 sr cm^{-1}), and 19.85 mW/(m^2 sr cm^{-1}) for the 0.6 µm, 0.8 µm, and 1.6 µm channels, respectively. The factor $v(t)$ takes into account the varying distance of the Sun as a function of the day t of the year.

The atmospheric correction module is based on SMAC, the Simplified Method for the Atmospheric Correction of satellite measurements in the solar spectrum (Rahman and Dedieu, 1994). TOC reflectance values R_β are calculated from the TOA values $\hat{R}_\beta$ as

$$R_\beta = \frac{\tilde{R}_\beta}{1 + \tilde{R}_\beta S_\beta} \quad \text{with} \quad \tilde{R}_\beta = \frac{\hat{R}_\beta - T_\beta^{gas} R_\beta^{atm}}{T_\beta^{gas} T_\beta(\theta_s) T_\beta(\theta_v)} \, , \tag{14}$$

where S_β is the spherical albedo of the atmosphere, T_β^{gas} is the total gaseous transmission, R_β^{atm} the “atmospheric reflectance”, and $T_\beta(\theta_s)$ and $T_\beta(\theta_v)$ “atmospheric diffuse transmittance” in the solar and viewing directions as it is defined by Rahman and Dedieu (1994). These quantities, which characterize the atmospheric absorption and scattering processes, are calculated from information about the atmospheric constituents by means of parametrizations with simple analytic functions whose coefficients depend on the spectral response of the respective channel considered. For our application the relevant coefficients corresponding to the MSG 0.6 µm, 0.8 µm, and 1.6 µm channels were provided by Berthelot (2001). A continental aerosol type is assumed and the aerosol optical thickness at 550nm, τ_{aer}, is currently specified according to a latitude dependent climatology (Berthelot et al.,1994) of the form:

$$\tau_{aer} = 0.2 \left[\cos(lat) - 0.25\right] \cos(lat)^3 + 0.05 \quad , \tag{15}$$

which is implemented in the operational system as a static file, thereby making reference to MDAL (LSA-01) and MTAL (LSA-02) products.

Likewise, there exist AL products based on the aerosol optical depth at 550 nm issued from the MACC-II project (www.gmes-atmosphere.eu). This recent initiative disseminates in near-real conditions the aerosol content and other atmospheric products based on a transport model for atmospheric particles with dedicated identification of sources and sinks. In the LSA SAF system the MACC-II forecast which is the closest (within 6 hours) to the slot is the one retained to generate the AL products. Note that a continental type is still further considered for time being.

The TOC reflectance values for the three used channels are determined for all SEVIRI scenes and are available as an internal product in the LSA SAF system. In the following methodological discussion we assume that all atmospheric effects are correctly accounted for and we consider the obtained results as true bi-directional reflectance factor values. In practice inaccurate knowledge of the atmospheric composition as well as simplifications in the correction approach can introduce random as well as systematic uncertainties. This point is illustrated in the Validation Report (VR) document.

4.3 BRDF model inversion

The atmospheric correction carried out by SMAC provides a set of n reflectance measurements $R_{j\beta}$ $(j=1,\cdots,n)$ in different spectral channels β given at irregularly spaced time points t_j and varying discrete values of the view θ_{vj} and solar zenith angles θ_{sj} (see Figure 3 for an example case). In the algorithm a linear kernel-based directional reflectance model of the form shown in Equation (12) is applied separately to each spectral band. In the following the index β referring to the channel is omitted for simplicity.

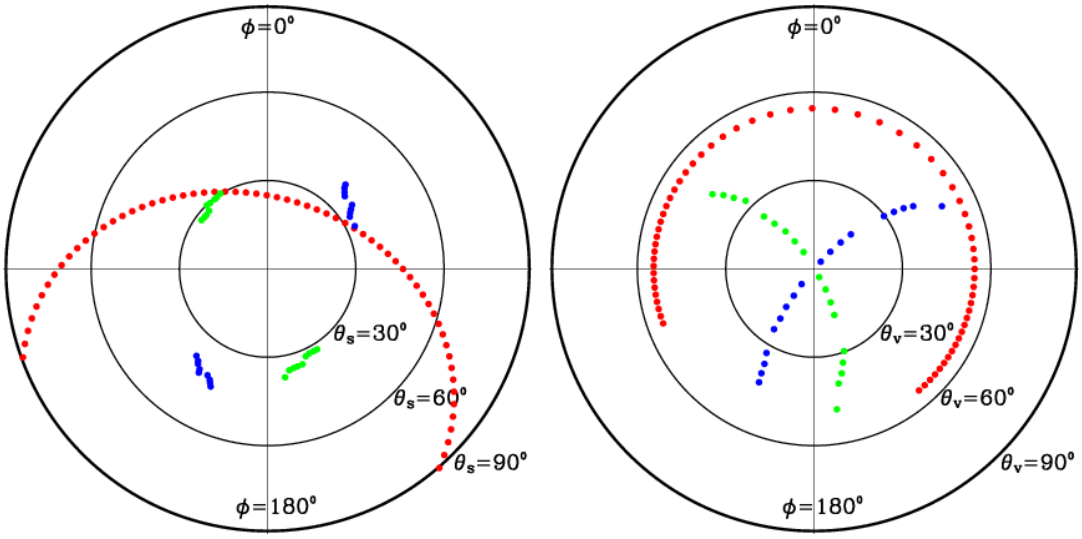

Figure 3: Illumination (left) and observation (right) geometries corresponding to a geographical location of [47° 47' N, 10° 37' E] and an observation period between the days of year 150 and 170. The relative azimuth angle φ is identical for the two graphs. The convention was chosen such that the top of the graphs (φ =0°) corresponds to the back scattering regime. The colors of the dots denote

observations taken by different sensors as follows: Red: SEVIRI/MSG, Green: AVHRR/METOP, Blue: AVHRR/NOAA.

The available TOC reflectance measurements provide the following system of n linear equations

$$R_j(\theta_{vj},\theta_{sj},\varphi_j)=\sum_{i=0}^{m-1} k_i f_i(\theta_{vj},\theta_{sj},\varphi_j)\ \ (j=1,\cdots,n)\ , \tag{16}$$

for constraining the m model parameters $k_i\ \ (i=0,\cdots,m-1)$. Introducing the vectors $\mathbf{k}=(k_0,k_1,\ldots,k_{m-1})^T$ and $\mathbf{R}=(R_1,R_2,\ldots,R_n)^T$, and the (n,m)-matrix $\mathbf{F}$ with the elements $F_{ji}=f_i(\theta_{vj},\theta_{sj},\varphi_j)$, allows us to rewrite the equation system in its matrix form:

$$\mathbf{R}=\mathbf{F}\,\mathbf{k}\ . \tag{17}$$

In general the number of available observations is larger than the number of unknown parameters and thus no exact solution for $\mathbf{k}$ exists. However, the observed reflectance is affected by measurement errors and therefore it is convenient to search for the best solution in a statistical sense and to quantify the uncertainties of the retrieved parameter estimates. In this case it may turn out that a considerably larger number of observations than parameters are required in order to reasonably constrain the parameter values.

The uncertainties of the individual reflectance factor measurements R_j are quantified by means of weight factors w_j, which are related to the inverse of the standard "1-sigma" uncertainty estimates $\sigma[R_j]$. We introduce the scaled reflectance vector $\mathbf{b}$ with the elements $b_j=R_j w_j$ and the "design matrix" $\mathbf{A}$ with the elements $A_{ji}=F_{ji}w_j$ (see e.g., Press et al., 1995). The linear least squares solution to the inversion problem in Equation can be found by solving the "normal equations"

$$(\mathbf{A}^{\mathbf{T}}\mathbf{A})\mathbf{k}=\mathbf{A}^{\mathbf{T}}\mathbf{b}\ , \tag{18}$$

for the parameters $\mathbf{k}$. The uncertainty covariance matrix of the retrieved model parameters is given by

$$\mathbf{C_k}=(\mathbf{A}^T\mathbf{A})^{-1}\ . \tag{19}$$

The diagonal elements C_{jj} of this matrix represent the variance $\sigma^2[k_j]$ of the respective parameters k_j. The covariance between k_i and k_j is given by the off-diagonal elements C_{ij}.

If the matrix $\mathbf{A}^T\mathbf{A}$ is far from being singular, the solution can be found by multiplying Equation "from the left" by the covariance matrix $\mathbf{C_k}$. In most of the cases this is feasible with a sufficient numerical accuracy. However, if a very small number of

measurements are available and the angular configuration is unfavorable (which is more likely to occur for geostationary satellite observations) the application of robust techniques involving singular value decomposition (SVD) and/or QR-decomposition is necessary to limit the effects of numerical errors when calculating the parameter estimates $\mathbf{k}=(k_0,k_1,k_2)^T$ and the uncertainty covariance matrix $\mathbf{C}_\mathbf{k}$.

To improve the result of the parameter estimation it can be useful to add constraints on the parameters themselves in the inversion of the linear model (e.g., Li et al., 2001; Hagolle et al. 2004; a related approach was also adopted by Pokrovsky et al. 2003). In the following we consider independent and uncorrelated a priori information on the parameters expressed in terms of the first and second moments (average and standard deviation, respectively) of their a priori probability distribution function, that is, an estimate of the form

$$k_i = k_{i\,\mathrm{ap}} \pm \sigma_{\mathrm{ap}}[k_i] \quad . \tag{20}$$

To simplify the notation let us consider an example with m =3 and an additional constraint for the two parameters k_1 and k_2. In this case adding the constraint of expression (20) to the equation system corresponds to extending the (n, m)-matrix $\mathbf{A}$ to the (n +2, m)-matrix

$$\mathbf{A}' = \begin{pmatrix} & \mathbf{A} & \\ 0 & \sigma_{\mathrm{ap}}^{-1}[k_1] & 0 \\ 0 & 0 & \sigma_{\mathrm{ap}}^{-1}[k_2] \end{pmatrix}, \tag{21}$$

and to extending the vector $\mathbf{b}$ to $\mathbf{b}'=(b_1,\ldots,b_n,k_{1\,\mathrm{ap}}\sigma_{\mathrm{ap}}^{-1}[k_1],k_{2\,\mathrm{ap}}\sigma_{\mathrm{ap}}^{-1}[k_2])^T$. The linear least squares solution with a priori information is then obtained in the same way as above by solving the normal equations.

More generally, taking into account a multivariate Gaussian a priori probability distribution function for the parameters quantified by its first and second moments corresponds to re-writing Equations and in the form

$$(\mathbf{A}^{\mathrm{T}}\mathbf{A}+\mathbf{C}_{\mathrm{ap}}^{-1})\mathbf{k} = \mathbf{A}^{\mathrm{T}}\mathbf{b}+\mathbf{C}_{\mathrm{ap}}^{-1}\mathbf{k}_{\mathrm{ap}}\,, \tag{22}$$

and

$$\mathbf{C}_\mathbf{k} = (\mathbf{A}^{\mathrm{T}}\mathbf{A}+\mathbf{C}_{\mathrm{ap}}^{-1})^{-1}, \tag{23}$$

with $\mathbf{k}_{\mathrm{ap}}=(k_{0\,\mathrm{ap}},\ldots,k_{m-1\,\mathrm{ap}})^{\mathrm{T}}$ and the covariance matrix $\mathbf{C}_{\mathrm{ap}}$. For uncorrelated a priori information on the parameters the matrix $\mathbf{C}_{\mathrm{ap}}=\mathrm{diag}(\sigma_{\mathrm{ap}}^2[k_0],\ldots,\sigma_{\mathrm{ap}}^2[k_m])$ is diagonal. Absence of a priori information on a given parameter – like it is the case for k_0 in the example case leading to the expression – corresponds to $\sigma_{\mathrm{ap}}[k_i]\to\infty$ and $\sigma_{\mathrm{ap}}^{-2}[k_i]\to 0$.

By adding constraints on m -1 model parameters, the inversion can be carried out with a minimum number of one available observation. In addition, the constraints on

the parameters reduce the condition number of the involved matrix and mitigate potential numerical problems. In practice we therefore add a regularization term corresponding to $k_1 = 0.03 \pm 0.05$ and $k_2 = 0.3 \pm 0.5$ which does not lead to a noticeable prejudice in the inversion result.

4.3.1 Surface BRDF model

In the following we restrict the discussion to a model with three parameters of the following form:

$$R(\theta_{out}, \theta_{in}, \varphi) = k_0 + k_1 f_1(\theta_{out}, \theta_{in}, \varphi) + k_2 f_2(\theta_{out}, \theta_{in}, \varphi) \; . \tag{24}$$

In the LSA SAF AL algorithm while k_0 quantifies an isotropic contribution to the reflectance factor $(f_0 = 1)$, functions f_1 and f_2 represent the angular distribution related to geometric and volumetric surface scattering processes, respectively. Roujean et al. (1992) suggest the following analytical expressions:

$$\begin{aligned} f_1(\theta_{out}, \theta_{in}, \varphi) = & \frac{1}{2\pi}[(\pi - \varphi)\cos\varphi + \sin\varphi]\tan\theta_{out}\tan\theta_{in} \\ & - \frac{1}{\pi}(\tan\theta_{out} + \tan\theta_{in} + \sqrt{\tan^2\theta_{out} + \tan^2\theta_{in} - 2\tan\theta_{out}\tan\theta_{in}\cos\varphi}) \; , \end{aligned} \tag{25}$$

(for $\varphi \in [0, \pi]$) and

$$f_2(\theta_{out}, \theta_{in}, \varphi) = \frac{4}{3\pi}\frac{1}{\cos\theta_{out} + \cos\theta_{in}}[(\frac{\pi}{2} - \xi)\cos\xi + \sin\xi] - \frac{1}{3} \; , \tag{26}$$

with the phase angle

$$\xi = \arccos[\cos\theta_{out}\cos\theta_{in} + \sin\theta_{out}\sin\theta_{in}\cos\varphi] \; . \tag{27}$$

Figure 4 depicts the dependence of these kernel functions on the zenith angle of the reflected light-ray for different illumination directions.

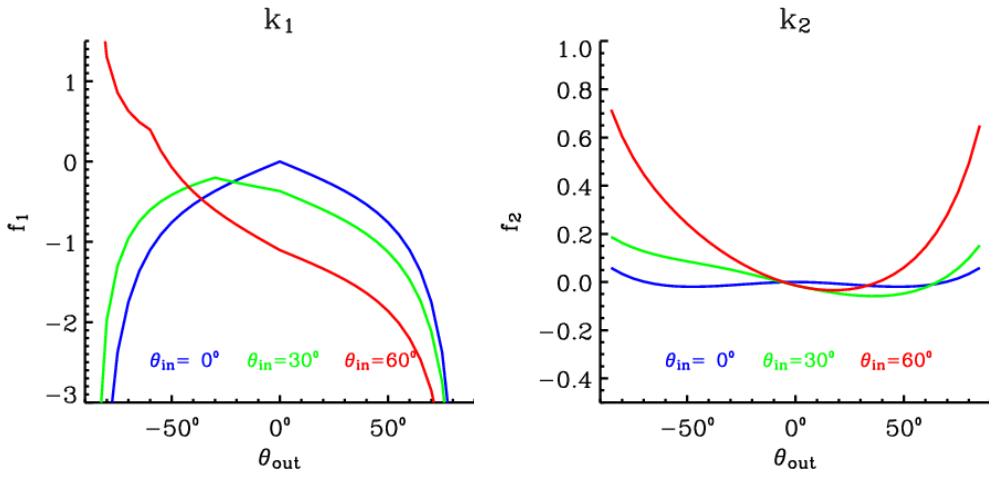

Figure 4: Angular dependence of the geometric (left) and volumetric (right) scattering kernels of the reflectance model introduced by Roujean et al. (1992). Negative zenith angle values correspond to the back scattering direction (relative azimuth angle φ =0°) and positive zenith angle values to the forward scattering direction (φ =180°).

4.3.2 Weighting of measurements

The matrix $F_{ji}=f_i(\theta_{vj},\theta_{sj},\varphi_j)$ is calculated knowing the angular configuration of each measurement point t_j . In order to determine the scaled reflectance vector $\mathbf{b}$ and the design matrix $\mathbf{A}$ it is necessary to specify the weight factors w_j . We choose an expression of the form

$$w_j=w_\theta(\theta_{vj},\theta_{sj})w_t(t_j)\ , \tag{28}$$

which simultaneously characterizes the angular as well as the temporal dependence of the weight attributed to each measurement point.

In the current configuration of the algorithm the temporal weight function

$$w_t(t_j)=1\ , \tag{29}$$

is kept constant since reflectance measurements for direct inversion are accumulated over a short composition period of one day only and the temporal composition of the daily observations is handled recursively as described in Section 4.3.4.

The angular component

$$w_\theta(\theta_{vj},\theta_{sj})=\frac{1}{\sigma[R_j(\theta_{vj},\theta_{sj})]}\ , \tag{30}$$

of the weight function is conveniently defined as the inverse of the estimated uncertainty of the reflectance measurements whose directional dependence is assumed to be a linear function of the relative air-mass $\eta(\theta_{vj},\theta_{sj})$:

$$\sigma[R_j(\theta_{vj},\theta_{sj})]=\sigma[R_j(\theta_v=0°,\theta_s=0°)]\,\eta(\theta_{vj},\theta_{sj})\ . \quad (31)$$

Estimates for the values of the reference uncertainties $\sigma[R_j(\theta_v=0°,\theta_s=0°)]$ at normalized geometry were obtained from a statistical analysis of atmospherically corrected SEVIRI scenes and are expressed as a linear function of the reflectance factor value

$$\sigma[R_j(\theta_v=0°,\theta_s=0°)]=c_1+c_2 R_j\ , \quad (32)$$

with coefficients for the three spectral bands as specified in Table 3. A lower limit of 0.005 and an upper limit of 0.05 are imposed to this quantity in order to avoid extreme values for reflectance outliers. A description of the method applied for obtaining the uncertainty estimates in a similar context is given in Geiger et al. (2005).

Table 3 - Coefficients for the parametrization of the TOC reflectance factor uncertainty estimates.

	0.6 µm	0.8 µm	1.6 µm
c_1	0.001	0.005	0.000
c_2	0.07	0.02	0.04

For the inversion process we take into account all reflectance observations whose solar zenith angle and view zenith angle do not exceed a threshold of 85°. In order to further decrease the weight for reflectance measurements taken at extreme angles close to this limit, the zenith angles are scaled in the calculation of the relative air-mass in the following way:

$$\eta(\theta_{vj},\theta_{sj})=\frac{1}{2}\left(\frac{1}{\cos\theta_{vj}}+\frac{1}{\cos\theta_{sj}}\right) \text{ with } \tilde{\theta}_{vj}=\theta_{vj}\frac{90°}{85°} \text{ and } \tilde{\theta}_{sj}=\theta_{sj}\frac{90°}{85°}\ . \quad (33)$$

The rationale of this prescription is the potential systematic problems in the atmospheric correction for very large solar and view angles, for which the employed scheme was not specifically designed, as well as the divergence of the f_1 geometric kernel function (cf. Figure 4).

In order to reduce the sensitivity to outliers due to undetected clouds, observations are eliminated from the analysis if the considered pixel is marked as cloudy in the CMa product in the slot acquired directly before or afterwards. In addition, observations for which the respective flag of the cloud mask product CMa indicates a bad quality are penalized in the weighting scheme by multiplying the reflectance uncertainty estimate by a factor 10. The same approach is adopted for the observations of pixels that might be contaminated by cloud shadows according to their location next to cloudy pixels and considering the solar azimuth direction. In this

way the potentially affected observations are only significant in the inversion process if no “reliable” observations are available at all.

4.3.3 Illustration of the model inversion

In order to illustrate the functioning of the model inversion approach, Figure 5 depicts an example for the series of atmospherically corrected reflectance factor values obtained from the SEVIRI image slots acquired during one day as a function of the solar zenith angle. The bars attached to each data point (from the center to each end) correspond to the uncertainty estimates used in the weighting scheme. Data points flagged as of bad quality in the cloud mask are marked in gray color. Image slots for which the considered pixel was flagged as cloudy are marked with a rhombus symbol at the abscissa. In this example this occurs for a number of slots close to local solar noon at a zenith angle of roughly 26°. The solid lines in the graphs represent the result obtained by re-calculating the reflectance factor with Equation from the retrieved best-fit model parameters in the same geometric configuration as the observations.

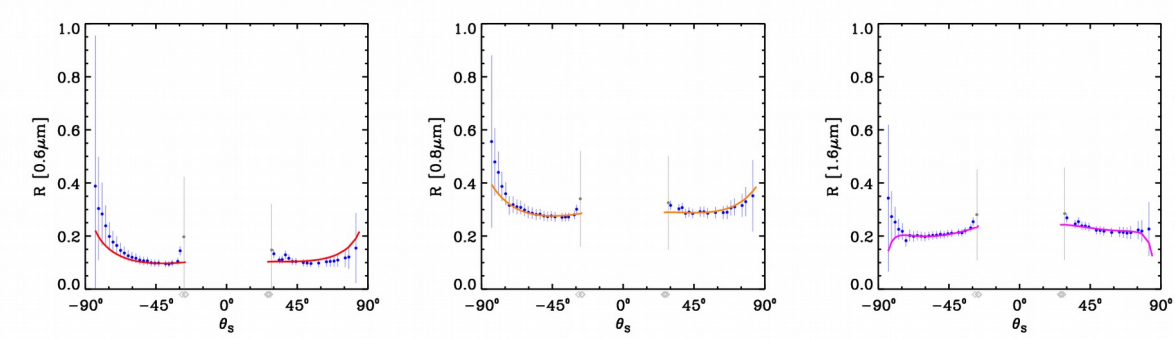

Figure 5: Example for the results of the TOC reflectance model inversion in the three used SEVIRI channels (49.02°N, 2.53°E; 1st of July 2006). Negative values of the solar zenith angles correspond to observations acquired before local solar noon.

The interest of the model fit for albedo determination is to obtain an interpolation and extrapolation of the reflectance factor for geometric configurations that are not observed. For one of the spectral channels of the example case, Figure 6 depicts the modeled reflectance factor for different illumination directions. The graphs illustrate that the angular dependence becomes increasingly important for large incidence angles.

The top and bottom panels of Figure 6 respectively show the principal and orthogonal planes which correspond to the vertical and horizontal sections of the polar graph shown on the right hand side of Figure 3. For the top panels negative values of the zenith angle θ_{out} correspond to the back scattering direction (φ =0°) and positive values to the forward scatter direction (φ =180°). The bottom panels, which are symmetric in θ_{out}, correspond to relative azimuth angles φ =90° and φ =270°.

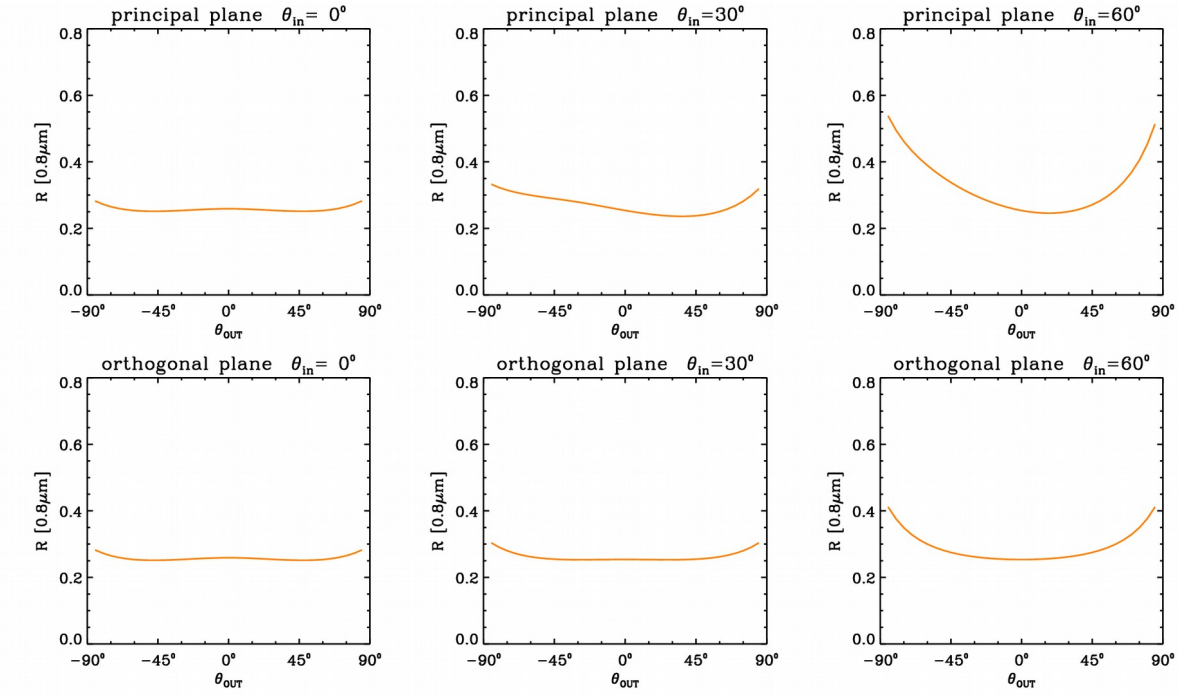

Figure 6: The dependence of the 0.8 μm-channel reflectance factor on the direction of the outgoing light ray for different incidence directions according to the model fit of the example case from Figure 5.

4.3.4 Temporal Composition

In order to reduce the sensitivity of the resulting daily estimates to reflectance outliers and extended periods of missing data because of persistent cloudiness, it is necessary to combine the information over a longer time period. A recursive scheme is applied for this purpose. At each execution of the algorithm the previous parameter estimate $\mathbf{k}_{\mathrm{in}}$ and the corresponding uncertainty measure $\mathbf{k}_{\mathrm{in}}$ is read from the relevant internal product files. Since these quantities now serve as input information, the index “in” is added to the symbols in order to distinguish them from the new estimates to be derived. The previous estimates are then used in the following way as a priori information for the linear model inversion specified in Equations and :

$$\mathbf{k}_{\mathrm{ap}} = \mathbf{k}_{\mathrm{in}}$$
$$\mathbf{C}_{\mathrm{ap}} = \mathbf{C}_{\mathbf{k}}^{\mathrm{in}} \left(1+\Delta\right)^{\left(t_0 - t_{\mathrm{in}}\right)/\Delta t} \text{ (with } \Delta t \text{ =1day).} \qquad (34)$$

The multiplicative factor (larger than one) applied to the covariance matrix reduces the confidence in the a priori estimate as a function of the lapse of time $t_0 - t_{\mathrm{in}}$ since the previous execution of the algorithm. The result of the inversion, constrained in this way with a priori information obtained from previous observations, is mathematically equivalent to performing the inversion directly with the complete set of observations by attributing less weight to those observations acquired before the day t_0 . A multiplicative factor in the weights translates into the inverse of the square

root of this factor in the elements of the covariance matrix resulting from the model inversion. The recursive multiplication process can therefore be identified with the presence of an effective temporal weight function [cf. Equation (28)] of the form

$$w_t(t) = (1+\Delta)^{-(t_0-t)/(2\Delta t)} \quad \text{for} \quad t \le t_0 \,, \qquad w_t(t) = 0 \quad \text{for} \quad t > t_0 \,, \tag{35}$$

which is shown in Figure 7. The quantity Δ can be related to the characteristic temporal scale τ (full width at half mean) of this weight function. This parameter is chosen as 5 days in the present configuration of the algorithm running in the operational system. When proceeding like this, it gives to past products a weight of 50% after 5 days and only 20% after 10 days. This value represents a satisfactory compromise between temporal resolution and sensitivity to remaining small scale variations in the reflectance factor values which are due to uncorrected atmospheric effects.

If no new observations are available during the whole day due to persistent cloudiness, the estimate for the model parameters $\mathbf{k}$ remains unchanged and only the multiplicative factor is applied for the covariance matrix as in Equation . The "age" of the last observation exploited in the recursive inversion scheme is an important piece of information for potential applications and is therefore also made available to the users.

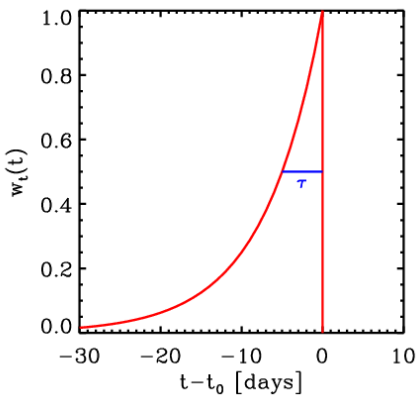

Figure 7: Effective temporal weight function in the recursive composition scheme. The characteristic time scale is τ = 5 days.

In line with the real-time strategy of LSA SAF the implemented method makes it possible to deliver the best estimate of the state of the land surface at the time of product generation and distribution by giving the largest weight to the most recent observations. At the same time owing to the successive accumulation of information a complete spatial coverage is achieved without the need for static surface information databases. Conceptually the implemented recursive composition scheme is similar to a Kalman filter without intrinsic time evolution of the model (cf. Samain, 2005).

4.4 Angular Integration

Inserting the reflectance model [Equation (12)] in the albedo definitions [Equations (5) and (6)] gives the expressions

$$a_\beta^{dh}(\theta_{\rm in}) = \boldsymbol{k}_\beta \boldsymbol{I}^{dh}(\theta_{\rm in}) \quad \text{and} \quad a_\beta^{bh} = \boldsymbol{k}_\beta \boldsymbol{I}^{bh} \ , \tag{36}$$

for the spectral albedo quantities, where

$$I_i^{dh}(\theta_{in}) = \frac{1}{\pi} \int_0^{2\pi} \int_0^{\pi/2} f_i(\theta_{out}, \theta_{in}, \varphi) \cos(\theta_{out}) \sin(\theta_{in}) \, d\theta_{out} \, d\varphi$$

$$\text{and} \quad I_i^{bh} = 2 \int_0^{\pi/2} I_i^{dh}(\theta_{in}) \cos(\theta_{in}) \sin(\theta_{in}) \, d\theta_{in} \ , \tag{37}$$

are the respective angular integrals of the fixed kernel functions which can conveniently be precomputed and stored in look-up tables. Figure 8 shows the illumination angle dependence of the directional-hemispherical integrals of the three kernels according to the model introduced by Roujean et al. (1992), which is currently used in the operational system.

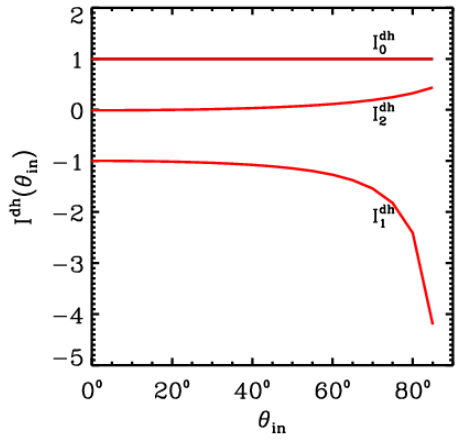

Figure 8: Illumination zenith angle dependence of the directional-hemispherical kernel integrals for the Roujean et al. (1992) model.

Thanks to the linear relationship [Equation (36)] between the BRDF model parameters and each of the spectral albedo quantities, standard uncertainty estimates for the latter can conveniently be derived from the respective uncertainty covariance matrix $\mathbf{C}_k$ of the model parameters (cf. Lucht and Lewis, 2000) and the appropriate kernel integrals $\mathbf{I}$:

$$\sigma[a]=\sqrt{\mathbf{I}^T \mathbf{C}_k \mathbf{I}} \quad . \tag{38}$$

Figure 9 shows the dependence of the directional-hemispherical albedo on the illumination zenith angle according to the result of the model fit for the example case discussed in Section 4.3.3. In the graphs an increase of a^{dh} with rising θ_{in} can be noticed which is characteristic for most types of land surfaces.

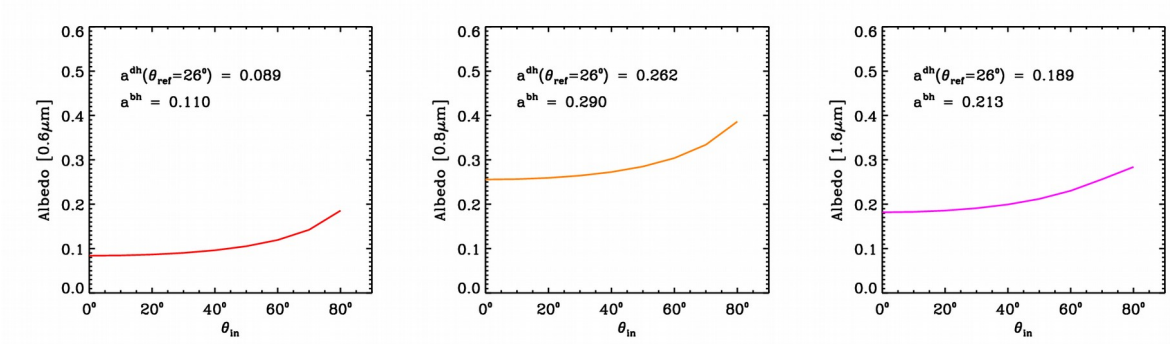

Figure 9: Dependence of the directional-hemispherical albedo on the illumination zenith angle for the example case from Figure 5. The value at the reference angle θ_{ref} and the bi-hemispherical estimate are indicated.

The LSA SAF albedo product files are the directional-hemispherical albedo $a^{dh}(\theta_{ref})$ for a specific reference angle θ_{ref} and the bi-hemispherical albedo a^{bh}. The solar position at local noon was chosen for the former product as the directional reference, which means that the zenith angle θ_{ref} is determined as a function of each pixel's geographic coordinates and the day of the year. For the time being the information on the complete functional dependence $a^{dh}(\theta_{in})$ is not available in the (external) product files. Appropriate empirical formulas (e.g., Dickinson 1983, Briegleb et al. 1986) may be applied for modeling the evolution of directional-hemispherical albedo $a^{dh}(\theta_s)$ according to the daily solar cycle. Finally, Equation (7) can be applied to calculate a weighted average of the directional and bi-hemispherical estimates as a function of the fraction of diffuse radiation in order to approximate a real sky situation.

As it can be seen from Figure 8, the directional-hemispherical integral $I_1^{dh}(\theta_{in})$ of the used kernel function f_1 tends to diverge as the illumination zenith angle approaches 90°. This may lead to a potential problem for the directional-hemispherical albedo when the illumination zenith angle is very large. However, the numerical values of the parameter k_1 are usually one order of magnitude smaller than k_2, which mitigates the apparent dominance of the f_1 kernel in the angular dependence of the integrals $I_i^{dh}(\theta_{in})$. In the algorithm an upper limit of 85° is specified for the reference angle θ_{ref} in the calculation of the directional-hemispherical albedo variant. Also, under such conditions the fraction of diffuse

radiation becomes dominant, and the directional-hemispherical albedo is then of little relevance for practical purposes. Owing to the weighting with the cosine of the illumination angle in the bi-hemispherical integral of Equation (37), the divergence of $I_1^{dh}(\theta_{in})$ is no problematic for the bi-hemispherical albedo variant.

4.5 Narrow- to Broad-band Conversion

The kernel approach offers a description of the angular dependence of the reflectance factor. It is applied to each instrument channel separately and provides no information on the spectral behavior outside of the available narrow bands. Broad-band albedo is defined as the integral of spectral albedo over a certain wavelength interval weighted by the spectral irradiance [cf. Equations (10) and (11)]. Since the integral can be approximated as a weighted sum of the integrand at discrete values of the integration variable, broad-band albedo may be expressed as a linear combination of the spectral (or rather narrow-band) albedo values in the available instrument channels.

In the LSA SAF algorithm the broad-band albedo estimates for a given target interval γ are derived from the spectral quantities by applying a linear transformation of the form

$$a_\gamma = c_{0\gamma} + \sum_\beta c_{\beta\gamma} a_\beta \tag{39}$$

with coefficients $c_{0\gamma}$ and $c_{\beta\gamma}$ as summarized in Table 4. Three different broad-band albedo intervals are considered: the total short-wave range from 0.3 µm to 4 µm, the visible wavelength range from 0.4 µm to 0.7 µm, as well as the near infrared range from 0.7 µm to 4 µm.

The narrow- to broad-band conversion coefficients were determined by van Leeuwen and Roujean (2002). Those authors performed a linear regression analysis based on radiative transfer simulations. They generated an extensive data set of synthetic spectral canopy reflectances for different surface types by using the ASTER spectral library (Hook, 1998) and the SAIL radiative transfer model (Verhoef, 1984). After calculating the narrow-band albedo values in the SEVIRI instrument's spectral bands and the broad-band albedo values in the ranges of interest, they then determined the corresponding linear transformation coefficients.

Table 4 - Narrow- to broad-band conversion coefficients for the SEVIRI channels (van Leeuwen and Roujean, 2002).

γ	$c_{0\gamma}$	$c_{1\gamma}$ (0.6 µm)	$c_{2\gamma}$ (0.8 µm)	$c_{3\gamma}$ (1.6 µm)
[0.3 µm, 4 µm]	0.004724	0.5370	0.2805	0.1297
[0.4 µm, 0.7 µm]	0.009283	0.9606	0.0497	-0.1245
[0.7 µm, 4 µm]	-0.000426	0.1170	0.5100	0.3971

The spectral properties of snow are rather different from those of ordinary land surfaces and the narrow- to broad-band conversion cannot be well described with the same linear relation. For pixels flagged as snow-covered in the CMa cloud mask product we therefore use the different set of coefficients listed in Table 5, which were determined with a similar regression analysis as described above.

Table 5 - Narrow- to broad-band conversion coefficients for pixels flagged as snow-covered calculated with tools developed by Samain (2005).

γ	$c_{0\gamma}$	$c_{1\gamma}$ (0.6 µm)	$c_{2\gamma}$ (0.8 µm)	$c_{3\gamma}$ (1.6 µm)
[0.3 µm, 4 µm]	0.0175	0.3890	0.3989	-0.0141
[0.4 µm, 0.7 µm]	0.0155	0.7536	0.2596	-0.5349
[0.7 µm, 4 µm]	0.0189	0.0942	0.5090	0.4413

The weighting with the spectral irradiance in the definition of the broad-band albedo introduces a dependence on the atmospheric conditions since the spectral properties of the incident solar radiation are different in clear and overcast sky situations. For the time being this difference is not taken into account in the generation of the input data sets for the regression analysis and the same narrow- to broad-band conversion relations are applied for the directional-hemispherical albedo $a^{dh}(\theta_{ref})$, irrespective of the reference illumination angle, and for the bi-hemispherical albedo variant.

Assuming that the errors of the spectral albedo estimates are uncorrelated, the uncertainty estimate for the broad-band albedo quantities is given by

$$\sigma[a_\gamma] = \sqrt{\sigma^2_{\text{Regression}} + \sum_\beta (c_{\beta\gamma})^2 \sigma^2[a_\beta]} \qquad (40)$$

where $\sigma^2_{\text{Regression}} = 0.01$ denotes the estimated residual variance of the linear regression.

4.6 Signification of the Uncertainty Estimates

The (theoretical) uncertainty estimates for the respective albedo quantities represent the most general quality indicator operationally delivered by the algorithm. They are calculated for each pixel as a function of the respective observation conditions. The validity of these estimates is strictly speaking restricted to the framework of the applied BRDF model and their quantitative pertinence needs to be checked with appropriate validation studies.

Determining the best solution of the linear model inversion problem in a least square sense implicitly includes the assumption that the probability distributions of the errors of the TOC reflectance factor values are Gaussian and mutually uncorrelated, that is their uncertainty covariance matrix $\mathbf{C_R} = \text{diag}(\sigma^2[R_1],...,\sigma^2[R_n])$ is diagonal. In practice correlated errors may occur owing to instrument calibration uncertainties and systematic biases in the applied atmospheric correction scheme (or in the

estimates of the concentration of atmospheric constituents used as input quantities for the correction). The uncertainty covariance matrix obtained for the model parameters therefore only quantifies the uncertainties due to the non-correlated (random) part of the input observation error structure.

When a large number of observations are available during clear periods the respective uncertainties for the model parameters become formally very small, which indicates that the model is then very well constrained. The albedo is calculated from the model parameters by linear expressions and the albedo uncertainty estimates are obtained by propagating those of the model parameters. Hence the albedo uncertainty estimates preserve the formal Gaussianity and they also reflect uncertainties due to the non-correlated part of the reflectance error structure while correlated (systematic) errors are not taken into account. The instrument calibration uncertainty may be taken into account a posteriori in a simplified way by “root-sum-squared-addition” to the delivered albedo uncertainty estimates.

With the implementation of the recursive temporal composition method, the uncertainty estimates also express the temporal aspect of the relevance of the observations. In periods without useful observations the uncertainty increases. This reflects the decreasing confidence in the parameter estimate due to “ageing” of the information on which the estimate is based.

Non-Gaussian outliers in the reflectance observations owing to undetected clouds cause another potential problem for the uncertainty treatment. Imperfections in the cloud screening method can lead to a significant contribution of outliers in the probability density distributions of the top-of-canopy reflectance errors. This can affect the quality of the inversion results as well as the validity of the uncertainty estimates. Nevertheless, the strategies employed for penalizing or eliminating potentially unreliable observations reduce the importance of this problem.

5 Known issues and limitations

- The albedo product time series may still contain spurious variability on short time scales, which may be caused by atmospheric effects like residual contamination by cloud and aerosol. Bearing in mind possible lack of appropriate information on aerosol characteristics (load and type), this has justified recently the project endeavor to produce two AL products using different aerosol inputs (MODIS satellite climatology and MACC-II forecast). In fact, MACC-II project appears to offer the necessary long-term perspectives to yield an improvement of the aerosol optical depth at 550 nm. Therefore, an even more positive impact on the accuracy assessment of the land surface albedo is reasonably foreseen is the near future. Besides, MACC-II re-analysis (from 2003) could be considered by the time of a LSA SAF products reprocessing. It is worth mentioning that forecast and analysis are close products in terms of quality.
- Around winter solstice the product quality at high Northern latitudes is reduced due to the low solar elevation angles. In mountainous areas during this period artifacts on the pixel scale caused by shadows can also occur.
- Solar eclipses are not taken into account and can perturb the product quality.
- The quality of AL products is appraised through a comparison with independent sources of validation like tower flux measurements. But marked differences in footprint sizes sometimes does not permit to conclude. Neither a robust conclusion is reached from comparing with other satellite-based products like MODIS and POLDER. This would suppose these latter stand for unbiased reference products. In fact elements of comparison – particularly differences versus specifications – should be regarded with caution. This is particularly the case over bright targets (desert, snow) where most satellite polar systems distribute reflectance values possibly in error due to large uncertainty on aerosol removal. For further information and details, we refer the reader to Validation Report (SAF/LAND/MF/VR_AL/II_2011).

6 References

Barnsley M.J., Strahler A.H., Morris K.P., and J.P. Muller, 1994, *Sampling the surface bidirectional reflectance distribution function (BRDF): Evaluation of current and future satellite sensors*, Remote Sensing Reviews, 8, 271-311.

Berthelot B., Dedieu G., Cabot F., and S. Adam, 1994, *Estimation of surface reflectances and vegetation index using NOAA/AVHRR: Methods and results at global scale*, Communications for the 6th International Symposium on Physical Measurements and Signatures in Remote Sensing, Val d'Isère, France, Jan. 17-21, 1994.

Berthelot B., 2001, *Coefficients SMAC pour MSG*, Noveltis Internal Report NOV-3066-NT-834.

Briegleb B.P., P. Minnis, V. Ramanathan, and E. Harrison, 1986, *Comparison of Regional Clear-Sky Albedos Inferred from Satellite Observations and Model Computations*, Journal of Applied Meteorology, 25, 2, 214-226.

Derrien M., 2002, *Specifications Calibration SEVIRI*, SPEC/MSG/001 v1.3, 2002, Météo-France/CMS.

Dickinson R.E., 1983, *Land surface processes and climate – Surface albedos and energy balance*, Advances in Geophysics, 25, 305-353.

Diner D.J. et al. (16 authors), 1998, *Multi-angle imaging spectro-radiometer (MISR) instrument description and experiment overview*, IEEE Transactions on Geoscience and Remote Sensing, 36, 1072-1087.

Ferranti, L. e P. Viterbo, 2006: The European Summer of 2003: Sensitivity of Soil Water Initial Conditions. *J. Climate*, 19, 3659-3680.

Geiger B., Hagolle O., and P. Bicheron, 2005, *CYCLOPES-Project: Directional Normalisation, Algorithm Theoretical Basis Document,* version 2.0.

Hagolle O., Lobo A., Maisongrande P., Cabot F., Duchemin B., and de Pereyra A., 2004, *Quality assessment and improvement of temporally composited products of remotely sensed imagery by combination of VEGETATION 1 & 2 images,* Remote Sensing of Environment, 94, 172-186.

Hook S. J., 1998, ASTER Spectal Library. http://speclib.jpl.nasa.gov

Hu B., Lucht W., Li X., and A.H. Strahler, 1997, *Validation of kernel-driven models for global modeling of bidirectional reflectance*, Remote Sensing of Environment, 62, 201-214.

Justice C.O. et al. (23 authors), 1998, *The Moderate Resolution Imaging Spectroradiometer (MODIS): Land remote sensing for global change research*, IEEE Transactions on Geoscience and Remote Sensing, 36, 1228-1249.

van Leeuwen W. and J.-L. Roujean, 2002, *Land surface albedo from the synergistic use of polar (EPS) and geo-stationary (MSG) observing systems. An assessment of physical uncertainties*, Remote Sensing of Environment, 81, 273-289.

Leroy M., Deuzé J.L., Bréon F.M., Hautecoeur O., Herman M., Buriez J.C., Tanré D., Bouffiès S., Chazette P., and J.L. Roujean, 1997, *Retrieval of atmospheric properties and surface bidirectional reflectances over the land from POLDER/ADEOS*, Journal of Geophysical Research, 102(D14), 17023-17037.

Li X., Gao F., Wang J., and A. Strahler, 2001, *A priori knowledge accumulation and its application to linear BRDF model inversion*, Journal of Geophysical Research, 106(D11), 11925-11935.

Lucht W. and P. Lewis, 2000, *Theoretical noise sensitivity of BRDF and albedo retrieval from the EOS-MODIS and MISR sensors with respect to angular sampling*, International Journal of Remote Sensing, 21, 1, 81-98.

Lucht W. and J.L. Roujean, 2000, *Considerations in the parametric modeling of BRDF and albedo from multiangular satellite sensor observations*, Remote Sensing Reviews, 18, 343-379.

Mitchell, K., et al., 2004: The multi-institution North American Land Data Assimilation System NLDAS: Utilizing multiple GCIP products and partners in a continental distributed hydrological modeling system, *J. Geophys. Res.*, 109, doi:10.1029/2003JD003823.

Pinty B., Roveda F., Verstraete M.M., Gobron N., Govaerts Y., Martonchik J.V., Diner D.J., and R. A. Kahn, 2000a, *Surface albedo retrieval from Meteosat. 1. Theory*, Journal of Geophysical Research, 105(D14), 18099-18112

Pinty B., Roveda F., Verstraete M.M., Gobron N., Govaerts Y., Martonchik J.V., Diner D.J., and R. A. Kahn, 2000b, *Surface albedo retrieval from Meteosat. 2. Applications*, Journal of Geophysical Research, 105(D14), 18113-18134

Pokrovsky I.O., Pokrovsky O.M., and J.-L. Roujean, 2003, *Development of an operational procedure to estimate surface albedo from the SEVIRI/MSG observing system in using POLDER BRDF measurements*, Remote Sensing of Environment, 87, 198-242.

Press W. H., Teukolsky S. A., Vetterling W. T., and B. P. Flannery, 1992, *Numerical Recipes in Fortran*, Cambridge University Press.

Rahman H. and G. Dedieu, 1994, *SMAC: A simplified method for the atmospheric correction of satellite measurements in the solar spectrum*, International Journal of Remote Sensing, 15, 1, 123-143.

Roujean J.-L., M. Leroy, and P.-Y. Deschamps, 1992, *A bidirectional reflectance model of the Earth's surface for the correction of remote sensing data*, Journal of Geophysical Research, 97(D18), 20455-20468.

Samain O., 2005, *Fusion multi-capteurs de données satellitaires optiques pour la détermination de variables biophysiques de surface*, Ph.D.-Thesis, Université Paul Sabatier, Toulouse.

Schmetz, J., P. Pili, S. Tjemkes, D. Just, J. Kerkman, S. Rota, and A. Ratier (2002), An introduction to Meteosat Second Generation (MSG), *Bull. Amer. Meteor. Soc.*, *83*, 977-992.

Sellers P.J., Mintz Y., Sud Y.C. and A. Duldres, 1986, *Simple Biosphere (SiB) Model for Use Within General Circulation Models*, J. Atm. Sci., 43, 505-531.

Strahler A.H., 1994, *Vegetation canopy reflectance modeling - Recent developments and remote sensing perspectives,* Proceedings of the 6th International Symposium on Physical Measurements and Signatures in Remote Sensing, 593-600.

Strahler A.H., Muller J.P. et al. (21 authors), 1999, *MODIS BRDF/Albedo Product: Algorithm Theoretical Basis Document,* version 5.0.

Trigo, I. F., C. C. DaCamara, P. Viterbo, J.-L. Roujean, F. Olesen, C. Barroso, F. Camacho-de-Coca, D. Carrer, S. C. Freitas, J. García-Haro, B. Geiger, F. Gellens-Meulenberghs, N. Ghilain, J. Meliá, L. Pessanha, N. Siljamo, A Arboleda (2010), The Satellite Application Facility on Land Surface Analysis, *Int. J. Remote Sens*., in press.

Verhoef W., 1984, *Light scattering by leaf layers with application to canopy reflectance modeling, the SAIL model*, Remote Sensing of Environment, 16, 125-141.

Wanner W., Li X., and A.H. Strahler, 1995, *On the derivation of kernels for kernel-driven models of bidirectional reflectance*, Journal of Geophysical Research, 100(D10), 21077-21090.

Wanner W., Strahler A., Hu B., Lewis P., Muller J.-P., Li X., Barker-Schaaf C., and M. Barnsley, 1997, *Global retrieval of BRDF and albedo over land from EOS MODIS and MISR data: Theory and algorithm*, Journal of Geophysical Research, 102(D14), 17143-17161.

Appendix A. Developers

The development and implementation of the albedo algorithm have been carried out under the responsibility of the Centre National de Recherches Météorologiques (CNRM) de Météo-France (MF).

Authors: Bernhard Geiger, Dominique Carrer, Olivier Hautecoeur, Laurent Franchistéguy, Jean-Louis Roujean, and Catherine Meurey

Appendix B. Glossary

AL: Land Surface Albedo Product
AVHRR: Advanced Very High Resolution Radiometer
BRDF: Bi-directional Reflectance Distribution Function
CNRM: Centre National de Recherches Météorologiques
CMa: Cloud Mask product developed by the NWC-SAF
cwv: column water vapour
CYCLOPES: Carbon Cycle and Change in Land Observational Products from an Ensemble of Satellites
ECMWF: European Centre for Medium-Range Weather Forecast
EPS: EUMETSAT Polar System
EUMETSAT: European Meteorological Satellite Organisation
HDF: Hierarchical Data Format
IM: Instituto de Meteorologia (Portugal)
NIR: Near Infrared Radiation
LSA: Land Surface Analysis
METEOSAT: Geostationary Meteorological Satellite
METOP: Meteorological Operational polar satellites of EUMETSAT
MISR: Multi-Angle Imaging Spectra-Radiometer
MF: Météo-France
MODIS: Moderate-Resolution Imaging Spectro-Radiometer
MSG: Meteosat Second Generation
NOAA: National Oceanic and Atmospheric Administration (USA)
NWC: NowCasting
NWP: Numerical Weather Prediction
POLDER: POLarization and Directionality of Earth Reflectance
SAF: Satellite Application Facility
SeaWifs: Sea-Viewing Wide-Field Sensor
SEVIRI: Spinning Enhanced Visible and Infrared Imager
SMAC: Simplified Method for the Atmospheric Correction
TOC: Top of Canopy
TOA: Top of Atmosphere
PRD: Product Requirements Document